Available online at www.sciencedirect.com

SCIENCE DIRECT®

Journal of volcanology and geothermal research

ELSEVIER

Journal of Volcanology and Geothermal Research 150 (2006) 300–312

www.elsevier.com/locate/jvolgeores

Mechanical discontinuities monitoring at Merapi volcano using kinematic GPS

F. Beauducel [a,c,*], M. Agung Nandaka [b], F.H. Cornet [c], M. Diament [c]

[a] *Observatoire Volcanologique et Sismologique de Guadeloupe – IPGP, Le Houëlmont, 97113 Gourbeyre, Guadeloupe FWI*
[b] *Merapi Volcano Observatory – BPPTK, Yogyakarta, Indonesia*
[c] *Institut de Physique du Globe de Paris, France*

Received 24 May 2004; received in revised form 26 January 2005; accepted 16 May 2005
Available online 18 January 2006

Abstract

Merapi volcano (Java, Indonesia) is in almost continuous activity with growth of an andesitic lava dome. This dome frequently collapses to form potentially deadly glowing avalanches, explosions and nuées ardentes. To monitor the evolution of surface displacements and to model the associated magmatic sources, we established a Global Positioning System (GPS) network in 1993 and have measured it each year using the static GPS method. However, the limited number of benchmarks and the geometry of the network did not allow us to precisely locate major mechanical discontinuities within the edifice. Precisely locating these discontinuities is of central importance because they delimit areas of potential instability and provide means to evaluate potential volumes of falling material.

The kinematic GPS method offers a way to partially solve the problem of temporal and spatial sampling of the displacement field, but its accuracy is usually insufficient to monitor small displacements. We propose here a strategy of field measurements and adjustments which combines kinematic positioning (1 min) and rapid static baselines (15 min) to get a 1.5-cm error (95% confidence). At Merapi summit, we have installed about 50 benchmarks covering the area around the main crater. Field measurements of this new network with our method take a few hours and the data processing has been automated.

We present the results of 8 surveys from 1999 to 2002, a period that includes a dome collapse in January 2001. Our results show large horizontal displacements towards the northwest, starting in July 2000 and reaching about 50 cm in amplitude in November 2000 that we interpret as precursors to the dome collapse. We also locate two presently active discontinuities at the summit of the volcano. This approach can be implemented easily on other active volcanoes.

Keywords: GPS; kinematic; lava dome; Merapi

1. Introduction

Forecasting eruptions and rock-slope instabilities on volcanoes requires evaluation of the location,

* Corresponding author. Observatoire Volcanologique et Sismologique de Guadeloupe – IPGP, Le Houëlmont, 97113 Gourbeyre, Guadeloupe FWI. Tel.: +33 590 590 99 11 38; fax: +33 590 590 99 11 34.
E-mail address: beauducel@ovsg.univ-ag.fr (F. Beauducel).

0377-0273/$ - see front matter © 2005 Elsevier B.V. All rights reserved.
doi:10.1016/j.jvolgeores.2005.07.005

extent, direction, magnitude and type (magmatic or phreatic) of deformation sources. This information is obtained by combining direct observations with an interpretative numerical model. The interpretive model needs boundary conditions (e.g., internal substructure geometries) and source parameters (pressure and stress field), which can be partially retrieved from an analysis of the deformation field.

The use of classic techniques of geodesy (e.g., GPS, tiltmeters, extensometers, distancemeters) leads to sparse data acquisition in time and space because of the limited number of sensors. Moreover imaging methods such as photogrammetry focus often on too small an area and are dependent on meteorological conditions. Satellite based remote-sensing techniques such as InSAR are not very well adapted for monitoring small areas such as lava domes. Furthermore, they are often difficult to use for monitoring purposes (availability of data, repeat time, loss of coherence). Deformation monitoring of small active areas, like lava domes, requires efficient techniques with sufficient spatial density and precision, and possibly 3-D positioning. The kinematic Global Positioning System (GPS) method (Genrich and Bock, 1992) can partially solve the problem of temporal and spatial sampling of the displacement field (Genrich et al., 1997; Bock et al., 2000; Baldi et al., 2000), but usually with insufficient precision to monitor small displacements. Because GPS has evident advantages for volcano monitoring applications, several data processing methods have been proposed to improve kinematic GPS resolution (Larson et al., 2001; Irwan et al., 2003). We present here a simple field protocol for measurement and adjustment that combines kinematic (1-min measurement sessions) and rapid static baselines (15-min measurement sessions). This method allows fast and simple surveys in areas that are not easily accessible, while producing results that are sufficiently accurate for efficient monitoring of volcanic edifices.

2. Merapi volcano

2.1. General background

Mt. Merapi (2964 m) is a young stratovolcano located in Central Java, Indonesia, in a frontal subduction zone (see Fig. 1). The population of Yogyakarta, an urban area located some 25 km from the summit, is about 3 million people including up to 500,000 that live directly on the flanks of the volcano above the 500 m elevation contour line. Mt. Merapi is one of the "Decade Volcanoes" as declared by the United Nations International Decade for National Disaster Reduction (IDNDR) Program (Voight et al., 2000a).

It is characterized by a quasi continuous extrusion of lava with an average rate of 3000 m^3/day over the last century (Voight et al., 2000b), and up to 300,000 m^3/day during episodes of unrest. Continuous growth of the dome inside a horseshoe shaped crater since 1961 has produced numerous glowing avalanches and Merapi-type pyroclastic flows (Bardintzeff, 1984) as a result of gravitational collapse.

2.2. Recent activity

Principal recent unrest episodes (lava dome growth or collapse with associated pyroclastic flows) of Merapi activity are (see Voight et al., 2000b for a complete review): February 1992, November 1994 (66 casualties), January 1997, July 1998, and January 2001. This last eruption was preceded by seismic activity that started in August 2000 (see Fig. 2) with volcano-tectonic and "multi-phase" shallow events, increasing in number until January 9, 2001. On January 10, 2001, the eruption started with numerous avalanches of lava until January 14, 2001, when the first pyroclastic flows occurred towards the southwest. From January 14 to mid-March 2001, about 1200 pyroclastic flows were observed, with a maximum rate of 71 events per day and a maximum run out of 6.5 km. Activity then decreased but started again between December 2001 and April 2002, producing tens of smaller pyroclastic flows. According to visual observations, a large part of the 1998 lava dome collapsed, and a new dome was emplaced at the same location (see Fig. 1).

2.3. Previous deformations studies

Merapi summit deformations have been monitored by American, Indonesian and French scientific teams using Electronic Distance Measurement (EDM) since 1988 and GPS measurements since 1993. Before the 1992 dome growth episode, Young et al. (2000) mea-

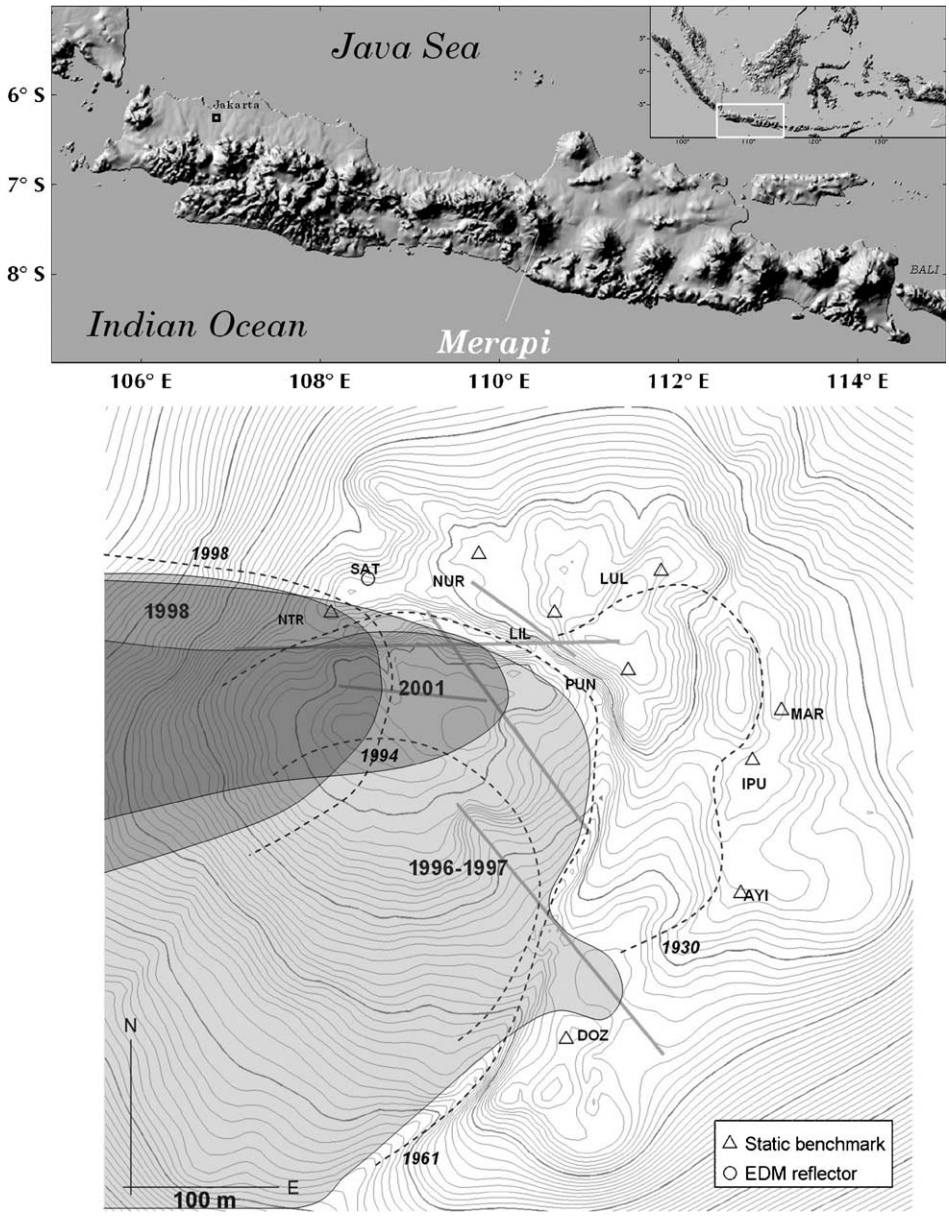

Fig. 1. Location of Mt. Merapi and topographic map of the summit (10-m contour lines). Approximate positions of main fractures (solid gray lines), areas of the lava domes (shaded with years in large type), and outlines of crater rims (dashed lines and year in italics) are also shown (modified after Sadjiman, 1992; Ratdomopurbo, 1995; Kelfoun, 1999; Beauducel et al., 2000).

sured horizontal displacements that reached 1.2 m/yr, associated with a strain rate of 11 ± 10^{-6}/day. Beauducel et al. (2000) conducted repeated GPS surveys from 1993 to 1997 and identified the main mechanical discontinuities of the summit structure through modeling with the 3-D mixed boundary elements method (Cayol and Cornet, 1997). Agung Nandaka (1999) continued the static GPS measurements from 1998 to 1999. Fig. 3 shows the cumulative horizontal GPS displacements for 1993–1999 at the summit. Despite the limited number of benchmarks, four zones separated by fractures with different behavior

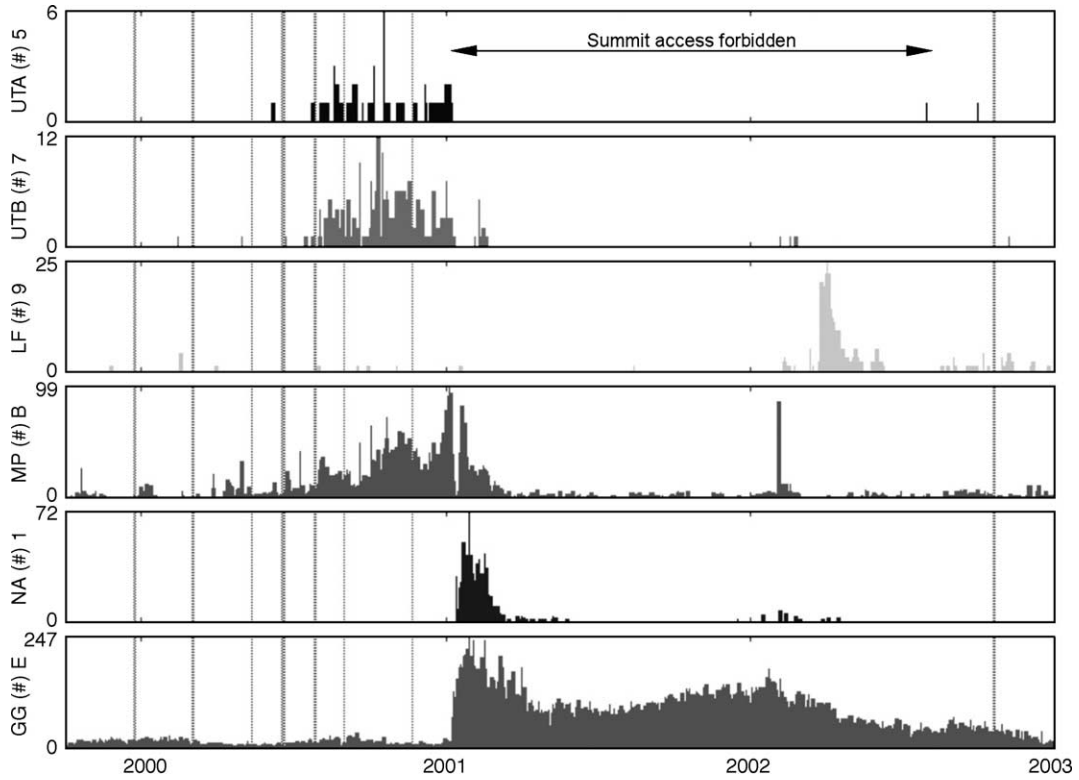

Fig. 2. Number of seismic events per day recorded between 1999 and 2002: VTA=volcano-tectonic >2 km deep, VTB=volcano-tectonic <1.5 km deep, LF=low frequency, MP=multi-phase (associated with magma production), NA=pyroclastic flows, GG=rock avalanches (source MVO). Dates for GPS surveys are also shown as dashed vertical lines.

are clearly evidenced. These fractures have been mapped in the field and introduced into the 3-D numerical modeling. The northwestern displacement at site NTR of about 55 cm was interpreted as a rock-slope instability potential, just before this zone collapsed in July 1998 (Beauducel et al., 2000).

Routine monitoring of deformation is achieved by EDM measurements between the Babadan observation post located some 4.5 km WNW from the summit and four reflectors installed on the western part of the summit. This provides frequent distance measurements on the most active part of the summit area. However, analysis of the deformation field is strongly limited by the small number of monitored points. Static GPS measurements at these 10 benchmarks take about 2 days with 2 receivers and 2-h occupations, and lead to position precisions of few mm (Beauducel et al., 2000). Because of the large displacements usually observed at the summit area before and during unrest episodes, we decided to increase the number of monitored points and to use a kinematic processing technique in order to decrease the survey duration, at the cost of a lower precision on the positioning.

3. Data acquisition and processing

3.1. Network setup

Considering the limited extent of the area of interest (a few hundreds of meters wide), we decided to set up a new network around the existing one. About 50 benchmarks were installed on the crater rim (Fig. 3), covering the whole accessible area with an average spacing of about 25 m. Some of the benchmarks are clustered around visible fractures (see Fig. 4a). Benchmarks consist of geodetic nails (10-cm long, 8-mm diameter, hollow head) fixed into massive lava blocks. Only the northern and eastern zones around the crater rim can be monitored, due to the steep topography

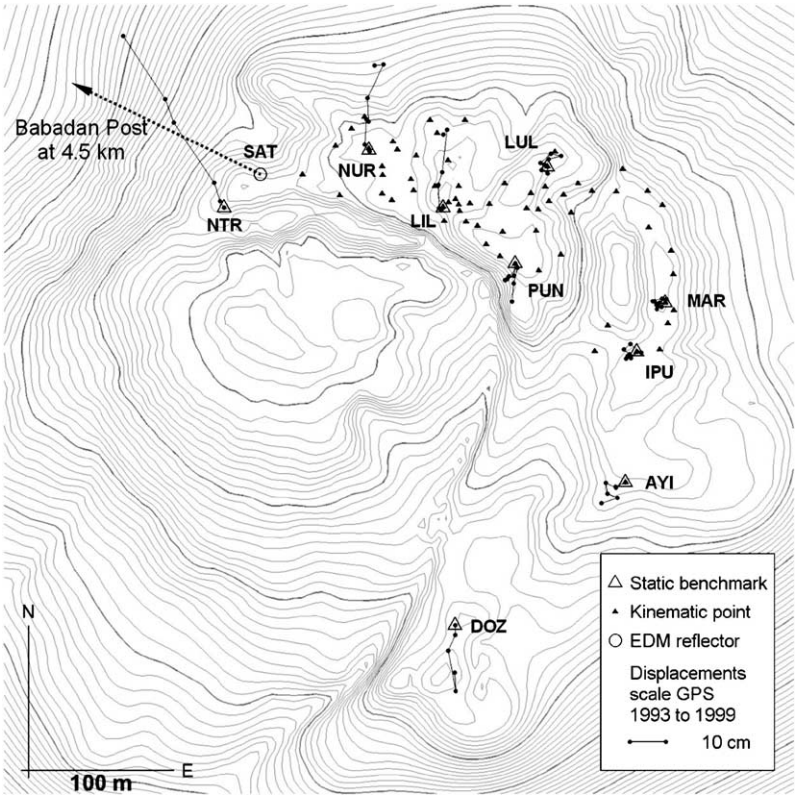

Fig. 3. Merapi summit GPS network: old benchmarks (large open triangles) and new kinematic points (small filled triangles, about 50 total). Location of EDM reflector SAT is also shown (large open circle). The direction to Babadan Post, located 4.5-km from the summit is given by the arrow. Cumulative horizontal static GPS displacements relative to September 1993 and measured during previous campaigns (September 1994, September 1995, September 1996, March 1997, March 1998, August 1998 and July 1999) are shown by black lines and points emanating from the open triangles (modified after Beauducel et al., 2000; Agung Nandaka, 1999). The DOZ benchmark became inaccessible starting end of 1997, and the NTR benchmark was lost during the July 1998 dome collapse.

elsewhere and because of the dome activity. The Southern zone is unfortunately too dangerous to access because of continuous rock-avalanche activity since 1997. The new network covers a 300×200 m area, with ellipsoidal elevations that range between 2926 and 2986 m.

The LUL point has been chosen as a reference station because of its stability over the last several years (Young et al., 2000; Beauducel et al., 2000) and its central position in the new network. This choice leads to a reduction of the length of the baseline trajectories.

Equipment consists in two *Dassault-Sercel Scorpio* dual-frequency receivers (see Fig. 4b), and the associated *3SPack* commercial software for post-processing. We use double-differenced phase measurements, L1 and L2 combination and Kalman filter solver for kinematic processing.

3.2. Methodology

The measurement method is illustrated in Fig. 5. The first receiver is set up at a reference point (A) and records at a 1-s sampling rate. A second receiver, with an antenna mounted on a 2-m-long pole, records continuously at the same sampling rate, and is moved along the new points and old benchmarks with a 2-min stop on each (see Fig. 4a). This trajectory is continuous and returns to the starting point in order to make a closed loop. It is repeated for redundancy. In the example shown on Fig. 5, two trajectories are measured in the following order: 1, 2, 3, B, 4, C, 5, 1, and 1, 2, 5, C, 4, 3, B, 3, 2, 1. Then, selected points of the trajectory are measured in a rapid-static mode, with 15-min measurements, to obtain precise baselines for A-B, A-C, and B-C.

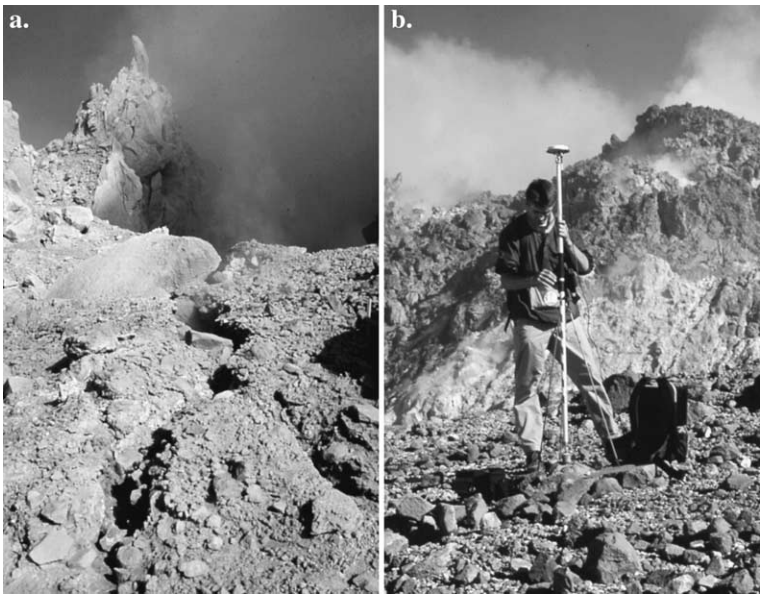

Fig. 4. (a) Surface evidence of fracture on the crater rim, near the NUR point (looking southeast). (b) Kinematic positioning on the AYI point (July 2000), with the active lava dome in background.

Trajectories are then post-processed in kinematic mode, and the coordinates of each benchmark, relative to reference point A, are extracted as the average of the 2-min measurement, as shown in Fig. 6. This leads to baseline components A-1, A-2, etc., with an approximate precision of 5 cm. Positioning errors increase with time and distance due to change in satellite constellation geometry. A large component of the uncertainty is also due to field difficulties: the 2-m pole has to be stabilized manually during the 2-min measurement using a small bubble level and a bipod. The operator may suffer some uncontrolled motion during windy weather. In contrast, rapid-static baselines yield a precision as low as 1 cm thanks to the short baseline length (<500 m) and the 15-min measurement duration at a 1-s sampling rate.

An important feature of our method is consideration of relative baselines in chronological order, e.g., A-1, 1-2, 2-3, 3-B, B-4, etc. This yields a better precision than considering long baselines A-2, A-3, etc., because the chronological baselines are very short (not more than a few tens of meters) and are separated in time by only few minutes. We then combine the kinematic baselines with the rapid-static ones to form closed loops within the network that can be adjusted and controlled to give the most precise measurements.

3.3. Network adjustment

All baselines are processed in the geocentric reference system (Cartesian) in order to avoid the effects of a local projection. Network adjustment is solved by the over-determined least squares linear system with known covariance

$$\mathbf{AX} \approx \mathbf{B} \tag{1}$$

$$\mathbf{X} = \left(\mathbf{A}^T\mathbf{V}^{-1}\mathbf{A}\right)^{-1}\mathbf{A}^T\mathbf{V}^{-1}\mathbf{B} \tag{2}$$

where

$$\mathbf{X} = \begin{pmatrix} \hat{x}_i \\ \hat{y}_i \\ \hat{z}_i \\ \hat{x}_{i+1} \\ \cdots \end{pmatrix} \tag{3}$$

is the vector of unknown points coordinates $\hat{x}$, $\hat{y}$, $\hat{z}$ (in the geocentric system),

$$\mathbf{A} = \begin{pmatrix} 1 & 0 & 0 & -1 & \cdots \\ 0 & 1 & 0 & 0 & -1 \\ 0 & 0 & 1 & \cdots & \cdots \\ \cdots & \cdots & \cdots & \cdots & \cdots \\ \cdots & \cdots & \cdots & \cdots & \cdots \end{pmatrix} \tag{4}$$

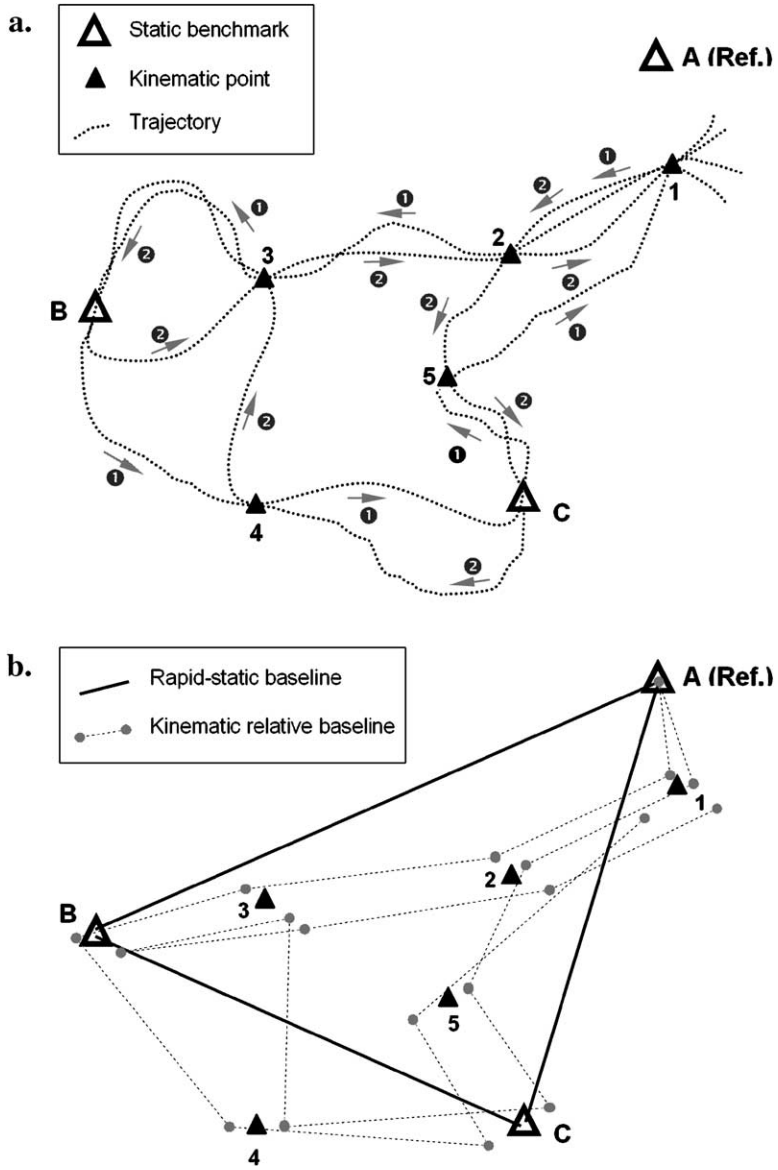

Fig. 5. Methodology: (a) Kinematic points (solid triangles), kinematic trajectories (dotted lines), and static benchmarks (outlined triangles). (b) Baseline results before network adjustment (exaggerated scale): Rapid-static baselines (solid lines), and kinematic relative baselines (dashed lines). Kinematic points are measured at least twice (2 min per measurement) as part of different trajectories starting with point 1 near the reference site A and ending at the same point (closed loops). These baselines have ~5 cm precision, and accumulated errors along the trajectory. At least 3 closed baselines are measured in rapid-static mode (15 min per measurement) between benchmarks common to different kinematic trajectories. These baselines have ~1 cm precision, and will control and adjust the network.

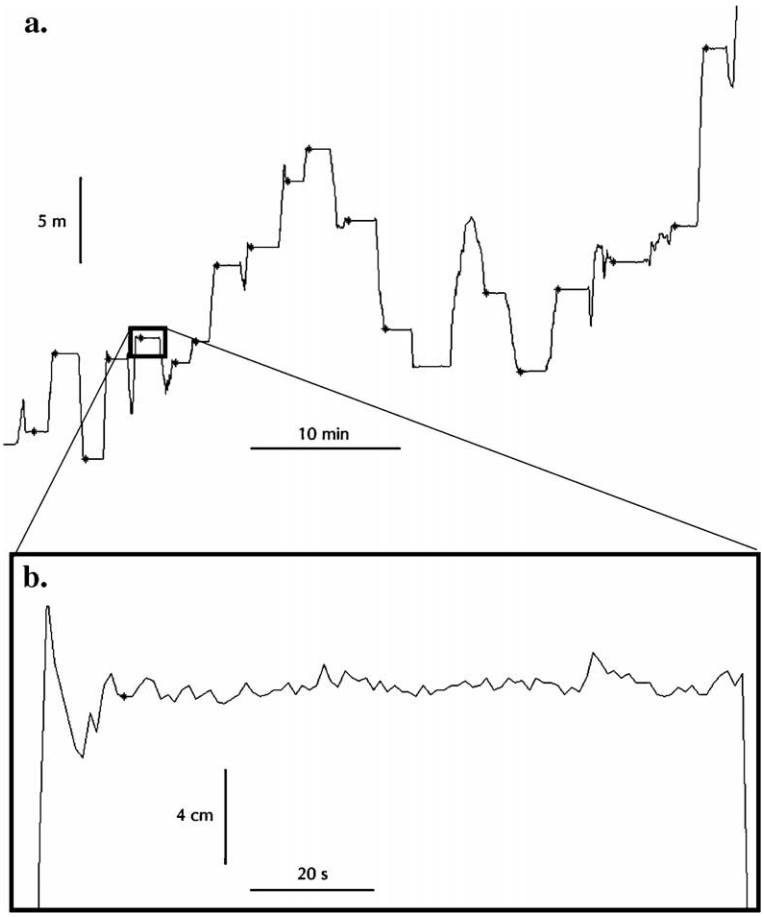

Fig. 6. Example of trajectory measurement and point position extraction: (a) vertical component versus time with stars indicating the onsets of point measurements; (b) enlarged portion of a 2-min measurement period shows a few centimeters of variation. The three components and uncertainties of kinematic baselines are computed as average and standard deviation of this time-period measurement.

is the matrix of partial derivatives,

$$\mathbf{B} = \begin{pmatrix} x_{i+1} - x_i \\ y_{i+1} - y_i \\ \dots \\ x_a - x_b \\ \dots \end{pmatrix} \tag{5}$$

is the matrix of observations (differential vectors components), and

$$\mathbf{V} = \begin{pmatrix} \sigma_x^2 & \sigma_{xy} & \sigma_{xz} & \dots & \dots \\ \dots & \sigma_y^2 & \sigma_{yz} & \dots & \dots \\ \dots & \dots & \sigma_z^2 & \dots & \dots \\ \dots & \dots & \dots & \dots & \dots \end{pmatrix} \tag{6}$$

is the covariance matrix associated with the observations. They are obtained from rapid-static post-processing and by averaging the standard deviation for kinematic points. The matrix **B** is constructed with chronological baselines (from point i to point $i+1$) for kinematic measurements, and site-dependent baselines (from point a to point b) for rapid-static measurements. The coordinates of the reference point are fixed.

Rapid-static baselines are adjusted in the standard way of geodetic network compensation. Because they have lower uncertainties, they control the precision of kinematic relative baselines when adjusting point positions. In this way, kinematic baselines are linearly "deformed" between each control point

Table 1
GPS survey details: date intervals, number of measured points, number of baselines (from kinematic and rapid-static measurements), and a posteriori RMS errors in the positioning (eastern, northern, and vertical components)

Survey dates	Nb of points	Nb of baselines	Eastern RMS (m)	Northern RMS (m)	Vertical RMS (m)
1999-12-23 to 1999-12-24	46	68	0.018	0.015	0.005
2000-03-02 to 2000-03-03	33	45	0.013	0.011	0.001
2000-05-12	27	28	–	–	–
2000-06-18 to 2000-06-19	44	50	0.069	0.062	0.002
2000-07-27 to 2000-07-28	54	101	0.023	0.018	0.010
2000-08-31	36	48	0.019	0.016	0.001
2000-11-21	32	36	0.030	0.032	0.001
2002-10-20 to 2002-10-21	50	193	0.009	0.007	0.004

The network adjustment inversion is controlled by (3 * points) number of unknowns, and (3 * baselines) number of data.

(redundant positioning, cross trajectories, and common static and kinematic points). A posteriori errors on the coefficients **X** are given using standard statistical formulae used for solving the least squares system (Eq. (2)).

Positions **X** and a posteriori errors are then projected in the Universal Transverse Mercator local reference coordinate system (UTM49). Finally, we computed differential displacement vectors from one survey to another. In order to process data within a few hours of the field survey, automatic *Matlab* routines have been written (Florsch, 2000) to produce numerical and graphical results, which can be taken into account for monitoring the volcano and assessment of hazards.

4. Results 1999–2002

The new kinematic GPS network was set up in December 1999, and measured using two receivers in March, May, June, July, August and November 2000. Due to unfavorable field conditions, some points could not be repeatedly measured in all surveys. After a long period during which access to the summit was forbidden because of the on-going eruption, field surveys started again in October 2002 (see Table 1) with two additional receivers. As a result we were able to measure the network with two different teams working simultaneously, significantly increasing the number of trajectories and baselines. Fig. 7 presents the relative displacement vectors computed from December 1999 to March 2000, July 2000, November 2000, and October 2002.

4.1. December 1999 to March 2000

During this period (Fig. 7a), we did not observe any significant displacements. The global RMS on uncertainties equals 0.85 cm, which proves that small motions can be detected. In addition, this establishes the efficiency of this method. Surprisingly, RMS errors are lower for the vertical component (0.4 cm) than for horizontal ones (1.2 cm). This is due to the use of a 2-m-high pole for the antenna. The pole is positioned on the nail; it cannot move vertically but it may slightly move horizontally due to motion of the operator. Indeed, a 1° movement of the pole corresponds to a 3.5-cm horizontal shift at the antenna top. The use of a conventional tripod would reduce the horizontal errors but would also significantly increase the duration of the survey. Since our objective was to carry out fast and light surveys, we decided to keep the described measurement protocol.

Fig. 7. Displacements and uncertainties (95%) relative to positions in December 1999. Numerical values correspond to vertical displacements in cm. Dashed lines indicate fractures. (a) March 2000: No significant displacements observed. (b) July 2000: the western and eastern zones are clearly separating (maximum 10 cm since December 1999) as also suggested by an active fracture oriented N20°E (dashed line). A known fracture (named Lava 56, oriented N80°E) shows a right-lateral slip of about 3 cm. (c) November 2000: The northwestern zone has moved up to 30 cm since December 1999. The anomalous motion northeast of the reference point appears to be caused by benchmark instability. (d) October 2002: Up to 80 cm of displacement since December 1999.

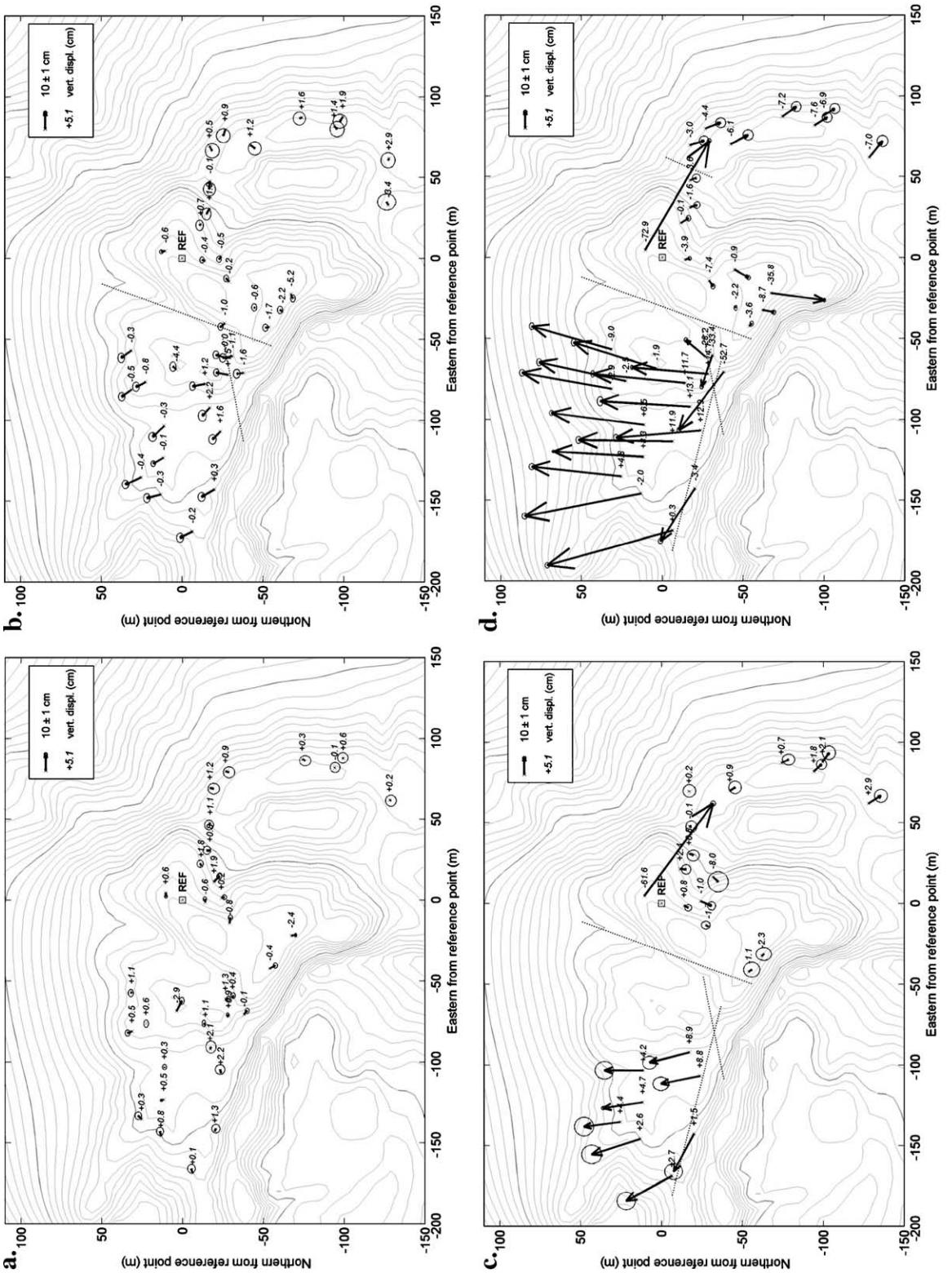
a.
b.
c.
d.
10 ± 1 cm
+5.1 vert. displ. (cm)
REF
Northern from reference point (m)
Eastern from reference point (m)

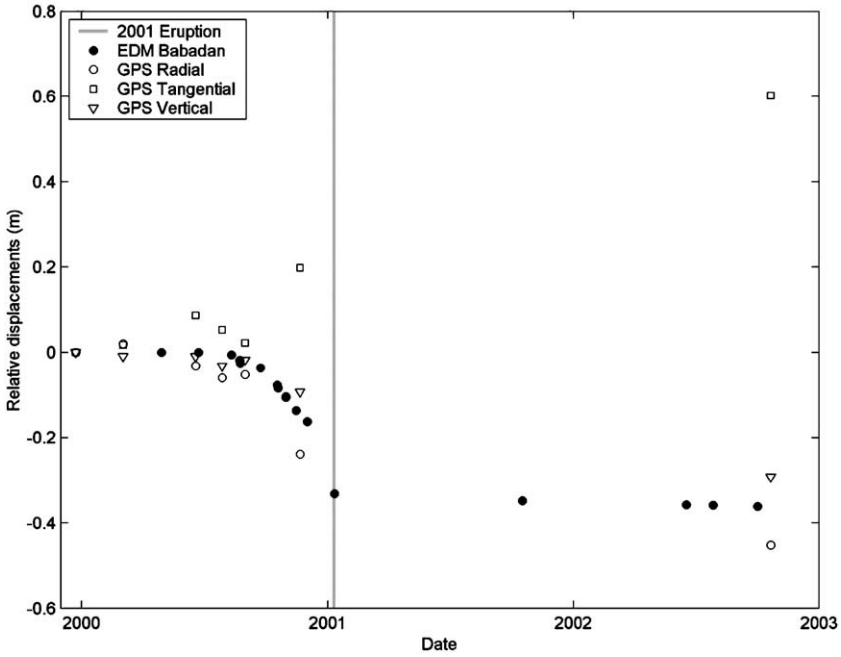

Fig. 8. Comparison of EDM distance measurements (solid circles) from Babadan Post, and projection of the nearest GPS point displacements on the same baseline (open circles). The tangential (open squares) and vertical (open triangles) GPS components are also shown. Errors in the EDM measurements are about 3.5 cm. The GPS radial component closely approximates the EDM observations, while the tangential and vertical GPS components show up to 60 cm of displacement which is not detected by the one-dimensional EDM result.

4.2. December 1999 to July 2000

During this period (Fig. 7b) a clear deformation pattern was observed. The western part of the network moved northwest with an average displacement of 10-cm, suggesting opening between the western and eastern zones. This allowed for recognition of an active fracture with a N20°E orientation that we approximately located between measured points. In addition, a known fracture oriented N80°E (Beauducel et al., 2000) showed a right-lateral slip of about 3 cm. As a consequence, we installed about 10 new benchmarks in the active zone.

4.3. December 1999 to November 2000

During this period (Fig. 7c), displacements of up to 35 cm in magnitude occurred on the northwestern zone points, revealing substantial extension over the newly identified N20°E fracture. The southwestern area did not follow the main displacement direction of this zone. Its displacement contained a southern component suggesting that it was decoupled by another fracture. This fracture had already been observed at the surface (see Figs. 1 and 4b), but this new result allowed us to define more precisely its orientation (N110°E) and location. Interestingly, eastern points along the 1930 crater rim also exhibited displacements of about 10 cm towards the southeast. Global RMS was quite large (2.8 cm in average) due to field positioning difficulties during the November 2000 survey. Note also the large southeastern displacement of 80 cm, with a vertical downward component of 60 cm. We interpreted this as an isolated moving block that we later identified in the field. Stable points in the vicinity seem to confirm this interpretation.

4.4. December 1999 to October 2002

In the last period (Fig. 7d), we observed the same deformation pattern with horizontal displacements of 80 cm to the north for the western points, suggesting rigid block motion. Moreover, the displacement vec-

tors for the southwestern points also clearly differ from those of the northern block, confirming that the previously identified fracture oriented N110°E was located somewhere north of the southwestern points. In addition, the eastern part of the summit showed displacements of about 10 cm which suggest the existence of a discontinuity to the north of K. Mati crater. Development of this amount of displacement over a long time period of 2 years may indicate that some displacements occurred prior to the January 2001 dome collapse.

5. Discussion

The lack of data during the last time interval prevents an assessment of whether the observed displacements are due to pre-eruptive effects, post-eruptive effects, or to both. To answer this question, we compared our measurements with EDM observations obtained from the Babadan Post (located on the northwest flank) during the same time interval. One of the reflectors (SAT) is located about 20 m to the west of the western-most kinematic GPS point (see Fig. 3). Fig. 8 shows relative distance measurements at this point, as compared to projected GPS displacements on the Babadan-summit baseline. EDM variations and radial GPS components (circles) are consistent within uncertainties (3.5 cm for EDM data), and the approximately 10 cm difference between both values may be explained by the different locations of the points. Because GPS vectors are 3-D, we also reported variations in tangential and vertical components through time, e.g., the two components that are not detected by EDM. This suggests that distance measurements from Babadan cannot detect cumulative horizontal displacements to the North as large as 60 cm, i.e., the main component of the displacement field.

On the other hand, EDM measurements carried out during the 2001–2002 (while summit access was forbidden for GPS surveys) indicated about 20 cm of displacement between November 2000 and January 2001, and then remained stable until October 2002. This suggests that at least a component of the GPS displacements measured in October 2002 was due to precursory deformation.

6. Conclusion

Rock-slope monitoring in exposed areas like the Merapi summit requires a dense geodetic network and brief measurement campaign. The methodology we propose here reduces the time spent in the field while increasing the number of points that are monitored with acceptable errors on positioning. Uncertainties after joint adjustment (kinematic and rapid-static) are less than 1.5 cm for the entire network (about 50 points) for all 3 components. The method requires at least 2 trajectories and 3 rapid-static baselines (equivalent to a 1-day campaign) in order to be effective.

During the period of our investigation, significant displacements were observed starting in July 2000 which continued and accelerated through November 2000. This deformation anticipated the January 2001 dome collapse and may be associated with magma production. Kinematic GPS surveys of the high density network also revealed a major new discontinuity within the edifice and helped to refine the location of known fractures. Moreover, it revealed deformation in the area of a future dome collapse. This method may be easily implemented on other volcanoes that cannot be easily monitored, or in places where the amount of available equipment is limited.

Acknowledgments

The authors thank M. Poland, E. Calais, Ph. Jousset, W. Crawford, J.-C. Komorowski, and an anonymous reviewer for useful comments on the manuscript. This work was supported by the Délégation aux Risques Majeurs (French Ministry of Environment) and the Volcanological Survey of Indonesia in the framework of the French–Indonesian cooperation in volcanology. GPS receivers were provided to the MVO staff trough this cooperation. We are very grateful to A. Ratdomopurbo for its continuous support, and to MVO staff, French volunteers and K. Kelfoun for their participation in field campaigns. Special thanks to G. Florsh for developing the first Matlab graphic user interface, and J. Ammann for his help in GPS hardware tests and software developments. IPGP contribution 2029.

References

Agung Nandaka, M., 1999. Étude des déformations d'un volcan actif à dôme. Application au Merapi. DEA report, Institut de Physique du Globe de Paris, 52 pp.

Baldi, P., Bonvalot, S., Briole, P., Marsella, M., 2000. Digital photogrammetry and kinematic GPS applied to the monitoring of Vulcano Island, Aeolian Arc, Italy. Geophys. J. Int. 142, 801–811.

Bardintzeff, J., 1984. Merapi volcano (Java, Indonesia) and Merapi-type nuée ardente. Bull. Volcanol. 47, 433–446.

Beauducel, F., Cornet, F., Suhanto, E., Duquesnoy, T., Kasser, M., 2000. Constraints on magma flux from displacements data at Merapi volcano, Java. J. Geophys. Res. 105, 8193–8204.

Bock, Y., Nikolaidis, R., de Jonge, P., Bevis, M., 2000. Instantaneous geodetic positioning at medium distances with the Global Positioning System. J. Geophys. Res. 105, 28223–28254.

Cayol, V., Cornet, F., 1997. 3D mixed boundary elements for elastostatic deformation field analysis. Int. J. Rock Mech. Min. Sci. 34, 275–287.

Florsch, G., 2000. Apport du GPS cinématique à l'étude du champ de déformations au volcan Merapi. Internal Report, Ecole Nationale Supérieure des Arts et Industrie de Strasbourg, Strasbourg.

Genrich, J., Bock, Y., 1992. Rapid resolution of crustal motion at short ranges with the Global Positioning System. J. Geophys. Res. 97, 3261–3269.

Genrich, J., Bock, Y., Mason, R., 1997. Crustal deformation across the Imperial Fault: results from kinematic GPS surveys and trilateration of a densely-spaced, small aperture network. J. Geophys. Res. 102, 4985–5004.

Irwan, M., Fumiaki, K., Naoyuki, F., Shigeo, N., Hidehumi, W., Shinichi, S., Motoo, U., Eisuki, F., Koji, K., 2003. Rapid ground deformation of the Miyakejima volcano on 26–27 June 2000 detected by kinematic GPS analysis. Earth Planets Space 55, 13–16.

Kelfoun, K., 1999. Processus de croissance et de destabilisation des dômes de lave du volcan Merapi (Java Centrale, Indonésie). Doctorate Thesis, Univ. Blaise Pascal Clermont-Ferrand II, France, 261 pp.

Larson, K., Cervelli, P., Lisowski, M., Miklius, A., Segall, P., Owen, S., 2001. Volcano monitoring using the Global Positioning System: filtering strategies. J. Geophys. Res. 106, 19453–19464.

Ratdomopurbo, A., 1995. Étude sismologique du volcan Merapi et formation du dôme de 1994. Doctorate Thesis, Univ. Joseph Fourier Grenoble I, Grenoble, France, 208 pp.

Sadjiman 1992. Pola perkembangan rekahan di puncak Gunung Merapi 1992, perubahan morfologi kubah lava dan lokasi reflektor. Internal Report, Merapi Volcano Observatory, Yogyakarta, Indonesia.

Voight, B., Sukhyar, R., Wirakusumah, A., 2000a. Introduction to the special issue on Merapi volcano. J. Volcanol. Geotherm. Res. 100, 1–8.

Voight, B., Constantine, E., Siswowidjoyo, S., Torley, R., 2000b. Historical eruptions of Merapi volcano, Java, Indonesia. J. Volcanol. Geotherm. Res. 100, 69–138.

Young, K., Voight, B., Subandriyo, Sajiman, Miswanto, Casadevall, T., 2000. Ground deformation at Merapi volcano, Java, Indonesia: distance changes, June 1988–October 1995. J. Volcanol. Geotherm. Res. 100, 233–259.